

ProbRadarM3F: mmWave Radar based Human Skeletal Pose Estimation with Probability Map Guided Multi-Format Feature Fusion

Bing Zhu^{*†}, Senior Member, IEEE, Zixin He^{*}, Weiyi Xiong, Guanhua Ding, Jianan Liu, Tao Huang, Senior Member, IEEE, Wei Chen, Senior Member, IEEE, and Wei Xiang, Senior Member, IEEE

Abstract—Millimetre wave (mmWave) radar is a non-intrusive privacy and relatively convenient and inexpensive device, which has been demonstrated to be applicable in place of RGB cameras in human indoor pose estimation tasks. However, mmWave radar relies on the collection of reflected signals from the target, and the radar signals containing information is difficult to be fully applied. This has been a long-standing hindrance to the improvement of pose estimation accuracy. To address this major challenge, this paper introduces a probability map guided multi-format feature fusion model, ProbRadarM3F. This is a novel radar feature extraction framework using a traditional FFT method in parallel with a probability map based positional encoding method. ProbRadarM3F fuses the traditional heatmap features and the positional features, then effectively achieves the estimation of 14 keypoints of the human body. Experimental evaluation on the HuPR dataset proves the effectiveness of the model proposed in this paper, outperforming other methods experimented on this dataset with an AP of 69.9%. The emphasis of our study is focusing on the position information that is not exploited before in radar signal. This provides direction to investigate other potential non-redundant information from mmWave radar.

Index Terms—mmWave radar, probability map, positional encoding, radar heatmap, multi-format feature fusion, human skeletal pose estimation

I. INTRODUCTION

HUMAN pose estimation is an important task in computer vision. It is often completed by detecting or tracking the joint keypoint to gain skeletal framework of the human body. Algorithms of deep learning are used to enable computers to understand and predict human pose or behaviour. In the very

This work has been submitted to the IEEE for possible publication. Copyright may be transferred without notice, after which this version may no longer be accessible.

B. Zhu, Z. He and W. Xiong are with School of Automation Science and Electrical Engineering, Beihang University, Beijing 100191, P.R. China. Email: zhubing@buaa.edu.cn (B. Zhu); hezixin2001@buaa.edu.cn (Z. He); weiyixiong@buaa.edu.cn (W.Xiong).

G. Ding is with the School of Electronics and Information Engineering, Beihang University, Beijing 100191, P.R. China. Email: buaadgh@buaa.edu.cn

J. Liu is with Vitalent Consulting, Gothenburg, Sweden. Email: jianan.liu@vitalent.se.

T. Huang is with College of Science and Engineering, James Cook University, Cairns, Australia. Email: tao.huang1@jcu.edu.au.

W. Chen is with the School of Biomedical Engineering, The University of Sydney, Camperdown, NSW 2050, Australia. Email: wei.chenbme@sydney.edu.au.

Wei Xiang is with the School of Computing, Engineering and Mathematical Sciences, La Trobe University, Melbourne, Australia. Email: w.xiang@latrobe.edu.au.

^{*}Both authors contribute equally to the work and are co-first authors.

[†]Corresponding author.

first and most pioneer studies, researchers rely on acquiring and analysing human pose data from RGB cameras. However, in recent years, non-visual signals based sensing has received more attention as people are absolutely concerned about privacy in the context of technological advancement. These signals will not contain human facial information, visual photographs, etc. Human activity can be inferred while not exposing subjects to privacy risks by using radio frequency signals, such as WiFi [6], radar signal [28], etc. WiFi has a narrow band and does not have sufficient distance resolution, resulting in limited downstream tasks that can be accomplished. So, millimetre wave radar, a cost-effective and higher resolution approach of sensing, has become another mainstream research method of indoor sensing. Moreover, it was found in research that mmWave radar performs even better in low light or obscured conditions in the indoor sensing task. It has great potential to replace currently used cameras in practical sense.

MmWave radar, as a robust but low cost sensor, has been applied for environment perception in advanced driver-assistance system (ADAS) [15–17, 31–33] and cooperative intelligent transportation systems (C-ITS) [8] in recent years. There has been a lot of frontier research on mmWave radar to achieve human activity sensing tasks. However, there are still challenges. In the classical radar processing pipeline, many different levels of data representation exist. For human skeletal pose estimation, point clouds and heatmaps are the most widely used forms of data representation. However, point clouds generation relies on hand-crafted parameters, and the process of generating the point clouds itself loses the Doppler information and some of the position information. This leads to difficulties in capturing features of finer joints through point clouds. Generating heatmaps is often done using Fast Fourier transform (FFT) method [9], which can extract range, Doppler and Angle of Arrival (AoA) information from the raw radar signal to generate different types of heatmaps. However, much of the information in the heatmap is considered redundant and is not valued. A large number of pose estimation works lately have been realised by point cloud + neural network pipeline, or heatmap + neural network pipeline. Some studies have paid more attention to improve the deep learning capability of networks and algorithms when addressing the mmWave radar based precision problem. While the importance of capturing the information present in radar signal itself is neglected, which leads to the loss of a lot of effective information.

To tackle the inefficiencies in traditional heatmap-based methods, we propose a new method, constructing a efficient

feature extraction framework. Specifically, our method includes two feature extraction branches. One branch follows the traditional steps, employing the FFT method to generate heatmaps to extract range, Doppler, azimuth and elevation information from mmWave radar signals. The other branch proposes a probability map generation and positional encoding method to enhance the effective use of position information in radar signals. We propose a model for fusing probability guided positional features with traditional heatmap features, and the contributions of our work are summarised below:

- We present a mmWave radar based multi-format feature fusion model ProbRadarM3F for human skeletal pose estimation. The model is designed for raw mmWave radar signals, features are extracted from 2 branches: FFT branch and ProbPE branch. In ProbPE branch, probability maps are generated, based on which positional encoding method is introduced. This study represents the first attempt to extract additional positional features from mmWave radar signals to aid in pose estimation task, by using a probability map guided positional encoding approach. By fusing features in different format, the keypoint prediction accuracy gains a great increase. ProbRadarM3F can be a baseline for research and application of radar position information exploitation.
- In order to validate the effectiveness of ProbRadarM3F, we choose to conduct experiments on the HuPR dataset, which provides purely raw radar signals. The results show that the design of probability map guided positional encoding strategy greatly improves the recognition performance of the model and gives a great improvement in the precision of human skeletal pose prediction.

The subsequent sections of this paper are organised as follows: section II provides a comprehensive review of the research and methodology of mmWave radar for indoor sensing applications, especially for human skeletal pose prediction. Section III specifies the implementation of our proposed ProbRadarM3F model. In Section IV, we present the experiments of ProbRadarM3F on HuPR dataset and evaluate its results. The advantages of its pose prediction are demonstrated. Finally, we summarise our approach and findings, as well as suggest potential directions for follow-up research in Section V.

II. RELATED WORKS

A. Millimeter-Wave (mmWave) Radar Indoor Sensing

The field of millimeter-wave (mmWave) radar for indoor sensing has gained substantial advancements in recent years, driven by the growing demand for non-invasive, privacy-preserving technologies for human presence and activity detection. MmWave radar has its unique advantages for indoor sensing applications. Mmwave frequency has ability to penetrate non-metallic objects while providing high-resolution imaging capabilities [23]. More and more utility is becoming apparent for mmWave radar in through-wall sensing [37], human detection and recognition [35] and vital sign monitoring [12, 13, 25].

Initially, researchers used radar signal processing to extract waveform features, combining with the target's distance, orientation, altitude and motion information to perform some simple action classification tasks [18]. Later, some research has started to introduce more advanced technology like deep learning for more accurate indoor sensing project from basic mmWave radar data. For instance, Wang et al. proposed a sequence-to-sequence (seq2seq) 3D temporal convolutional network with self-attention method to estimate human hand pose [20]. Yi et al. utilize a multi-person detection model based on long short term memory (LSTM) to determine the presence of humans and localize their positions with a single 60GHz mmWave radio [34]. Wu et al. first put forward work to segment human silhouette from the millimeter wave RF signals. They locates human reflections on radar frames and extract features from surrounding signals with human detection module and extracted features from aggregated frames with an attention based mask generation module [29]. Although these studies have been highly successful, they have focused more on changes in the structure of the deep learning network and neglected how to extract more valid features from the radar signal. Given the inherent limitations of mmWave radar data, this oversight may result in the loss of valuable information during processing.

B. MmWave based Human Skeletal Pose Estimation

Since the application occasion has high demand of both privacy and precision, the advent of mmWave radar technology has markedly expanded the horizons of human pose estimation and recognition. One of the notable research directions in human pose estimation is the focus on skeletal pose recognition. The advantage of human skeletal pose estimation lies in its ability to provide a simplified yet informative representation of human pose and movements, facilitating efficient and accurate human activity recognition. Skeletal pose prediction derived from mmWave radar signals feature critical spatial and temporal information about human activity without the privacy concerns associated with optical imaging.

RF-Pose [36] is one of pioneering works which first considers human skeleton reconstruction. Zhao et al. proposed a deep network from FRCM signals to estimate coarse human skeleton parts under the supervision of visual information. Then they improved the model which successfully predict 14 human joints, including head, neck, shoulders, elbows, wrists, hip, knees, and feet. RF-Pose and its follow-up work used expensive customized hardware system, nowadays, more studies based on low-cost mass-produced industrial millimetre wave radar and has demonstrated good performance. Ding et al. presented a kinematic constrained learning architecture that incorporates the kinematics constraints with the learning of neural network for skeleton estimation of human body based on range-Doppler heatmaps [5]. Kong et.al performed a convolution operation on the Range-Doppler-Profile to detect human's corresponding ranges and design a two-stream deep learning architecture to extract the body shape and motion features to predict skeleton joints coordinates and reconstruct the body posture [10]. Cao et al. developed a model to

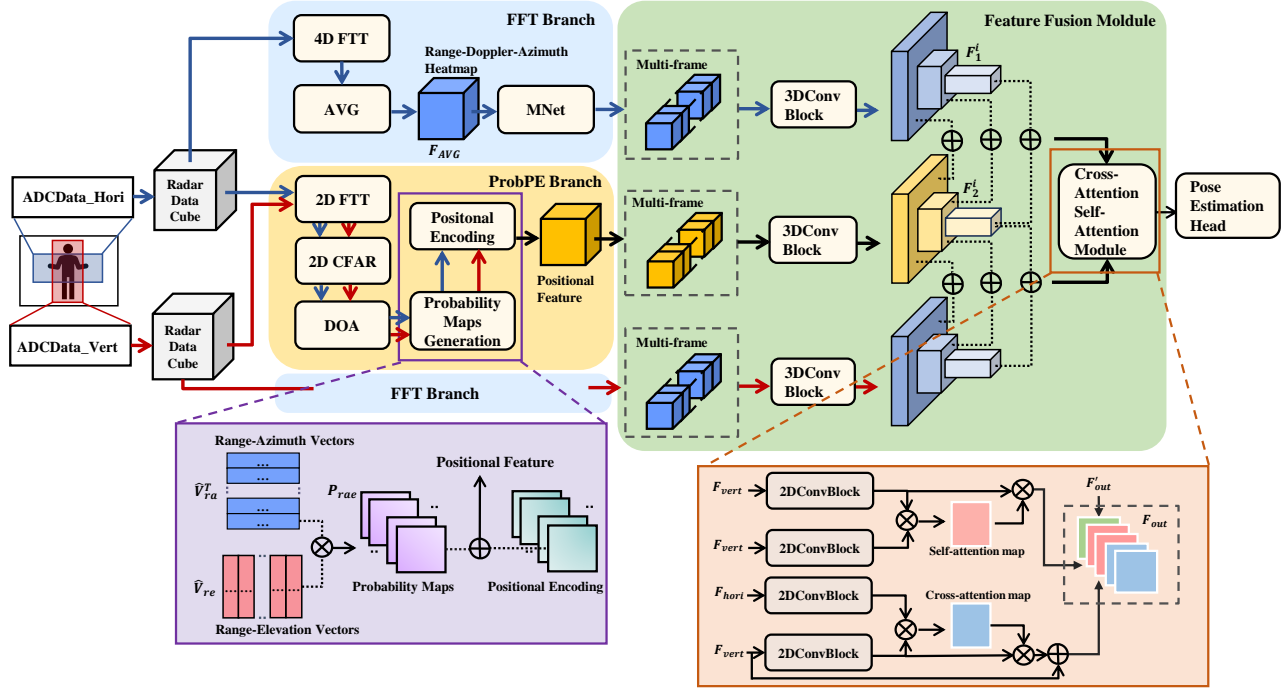


Fig. 1. Our proposed ProbRadarM3F model consists of two main branches. The initial input is the raw ADCdata from two vertically placed mmWave radar. Different coloured arrows represent data streams from different radars. After processing raw radar data into radar data cube, the FFT branch process the data to extract feature from range-Doppler-azimuth heatmaps and range-Doppler-elevation heatmaps based on 4D-FFT. ProbPE branch applies positional encoding to extract features from generated radar propability maps. In the following module, the multi-frame and multi-format features are fused and a cross- and self-attention module is introduced to generate skeletal pose estimation.

incorporate the part-level range-Doppler maps for individual body parts with the local kinematic constraints with the global constraints for reconstructing the human skeleton [2].

III. PROPOSED METHODS

In this section, we provide detailed descriptions of ProbRadarM3F for human skeletal pose estimation based on the fusion of multi-format feature from mmWave radar data. The structure of the model is illustrated in Fig. 1. After processing the raw signal from mmWave radar, the model respectively extract features from the radar data through the FFT branch and the ProbPE branch. Multi-frame features in different format from the two branches are fused, and finally we predict the coordinates of human skeletal joints from the fused features via a cross-self-attention mechanism.

A. FFT Branch: Radar Data Processing and Range-Doppler-Angle Map Generating

The dataset we used provides only unprocessed raw radar data acquired by the DAC1000 system. Therefore, we first pre-process the radar signal in order to converting the raw analogue-to-digital converter (ADC) data into a structured format, as a radar data cube, for efficient signal processing and analysis.

The raw ADC data captured in binary format is initially one-dimensional, representing interleaved ADC samples across

multiple channels. We structured it by organising the data into a two-dimensional matrix to separate the individual Low Voltage Differential Signaling (LVDS) channels. By segregating the samples from even and odd channels, we construct the real and imaginary components of the complex signal. This ensures the retention of phase information necessary for following processing tasks. Ultimately, the complex data is reformatted into a radar data cube to accurately reflect the sequence of radar data acquisition. This reorganization involves structuring the data into blocks that correspond to each chirp across multiple transmit (TX) and receive (RX) channels. The radar data cube accurately retains information about the spatial and temporal dimensions of the observed scene.

As shown of FFT branch in Fig. 1, we initiate a comprehensive analysis by performing a 4-dimensional FFT (4D FFT) along the four axes: ADC samples, chirps, horizontal antennas, and vertical antennas as following:

$$F(h, i, j, k) = \sum_{n=0}^{N-1} \sum_{m=0}^{M-1} \sum_{p=0}^{P-1} \sum_{q=0}^{Q-1} f(n, m, p, q) \times e^{-j2\pi(\frac{hn}{N} + \frac{im}{M} + \frac{jp}{P} + \frac{kq}{Q})} \quad (1)$$

where $f(n, m, p, q)$ is the original input signal across ADC samples n , chirps m , horizontal antennas p , and vertical antennas q and $F(h, i, j, k)$ is the results of Fourier transform. N, M, P, Q represent the sizes of the dimensions. h, i, j, k represent the indices in the frequency domain for the correspond-

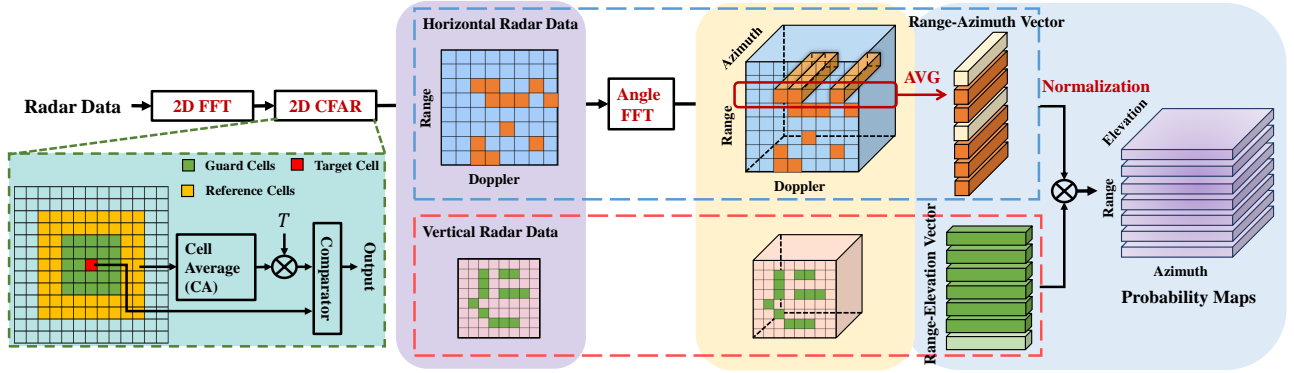


Fig. 2. The probability map is the guidance of the positional encoding method. Initially, the range bin is filtered out by performing 2D CFAR on the range-Doppler heatmaps. The angle information on the selected range is extracted, thus yielding the range-azimuth vectors and the range-elevation vectors. These vectors are normalized, transposed, and then multiplied to generate a probability maps, which respond to the probability of the target appearing at a certain position.

ing dimensions. This process yields detailed range-Doppler-azimuth-elevation maps. Moreover, we uniformly sample a certain amount of chirps within a specific velocity range in the Doppler dimension to filter out irrelevant information in the radar signal. This approach effectively filters out extraneous signal components, thereby streamlining the dataset for enhanced processing efficiency.

The dataset we used provides data collected by two vertically placed radars. Since the resolution and detection range of the adopted radars in elevation angle directions are limited, we average elevation information of each radar in the processing:

$$F_{avg} = \frac{1}{Q} \sum_{k_q=0}^{Q-1} F(k_m, k_n, k_p, k_q) \quad (2)$$

The azimuth information of the horizontally placed radar is retained, while the azimuth information of the vertically placed radar is considered as the elevation angle information on overall data. We eventually obtained the range-Doppler-azimuth map from the horizontal radar and the range-Doppler-elevation map from the vertical radar. To combine dynamic information across varying chirps within the range-Doppler-angle maps, we introduce M-Net [27] to merge features from multiple chirps into one. The M-Net module uses a neural network instead of the traditional method of fusing different chirp information within a frame to solve for Doppler velocities, outputting the merged features of the frame.

B. ProbPE Branch: Probability Map Generating and Positional Encoding

As it shown in Fig. 1, in ProbPE branch, after taking the radar data cube, we initially subject the input radar data cube to a two-dimensional FFT (2D FFT). The FFT is executed in the fast time dimension (the dimension of digitised chirp samples) to obtain range information. Given the significant impact of frequency effects of velocity in the slow time dimension—where multiple frames correspond to the same range unit—an FFT is also conducted in this dimension to obtain the Doppler frequency. To minimize irrelevant information

that could potentially increase computational load or interfere with feature extraction, we employ Constant False-Alarm Rate (CFAR) [19]. This is instrumental in distinguishing between targets and interference noise based on intensity disparities. We use 2-dimensional (2D-CFAR) on range-Doppler maps to select the elements that contains more valid information. In the 2D-CFAR detection process, in order to place the direct influence of potential targets on the noise estimation and to provide a reference for the dynamic threshold adjustment, the targets are detected as accurately as possible to reduce false alarms. Corresponding guard cells, and reference cells, are introduced in the vicinity of each detection cell, shown as in the lower left corner of Fig. 2. Cell Averaging CFAR (CA-CFAR) is a prevalent variant of CFAR, which employs the following formula to calculate the threshold for each cell under examination:

$$T = \alpha \cdot \frac{1}{N} \sum_{i=1}^N X_i \quad (3)$$

where T represents the threshold for the cell, X_i represents the amplitude values of the reference cells surrounding the cell under test, N represents the number of reference cells considered, and α is a scaling factor determined by the desired false alarm rate. If the intensity of the target surpasses that of interference noise, as $I_{target} > I_{noise} \times T$, it indicates the presence of the target.

Subsequently, probability maps are derived from the filtered range bins, which serve as a foundational step in understanding the spatial distribution of potential targets. It is noted that we take the concatenation set for the filtered range bins from the two radars separately. The phase differences among various antennas yield distinct spikes, denoting frequency components from different directions. Angle information is obtained by performing FFT on target data from distinct virtual antennas. We execute Angle FFT to derive azimuth from horizontal radar and elevation from vertical radar. We make an averaging calculation in the Doppler dimension because the focus at this point is on probability and position information. Thus, range-

azimuth and range-elevation vectors from the two radars are extracted, respectively. These vectors contain information on the radar's intensity at specific ranges and angles, effectively characterizing the probability of a target's presence at a given location. Consequently, we construct radar probability maps, illustrated as Fig. 2.

We proceed with the normalization of these vectors, ensuring uniformity in the data. Following normalization, we transpose and multiply the range-azimuth and range-elevation vectors at identical ranges to generate range-azimuth-elevation probability maps:

$$P_{\text{rae}}(r, \theta, \phi) = \hat{V}_{\text{ra}}(r, \theta)^T \cdot \hat{V}_{\text{re}}(r, \phi) \quad (4)$$

where $P_{\text{rae}}(r, \theta, \phi)$ represents the probability map indicating the likelihood of detecting a target at range r , azimuth θ , and elevation ϕ . $\hat{V}_{\text{ra}}(r, \theta)$ represent the normalized range-azimuth vector and $\hat{V}_{\text{re}}(r, \phi)$ denote the normalized range-elevation vector.

These maps not only indicate the probability of detected elements but also contain significant geometric information, suggesting further exploitable position information. In the landscape of advanced deep learning methodologies, the Transformer [24] introduces a sine coding formula for positional encoding, enhancing the model's spatial perception. DETR [3] incorporates the Transformer model into target recognition, applying sine positional encoding to 2D images. In our project, for each range r , the azimuth-elevation probability map can be treated as a two-dimensional representation, so we introduce sine positional encoding to extract positional information from the maps. The sine encoding formula is as follows:

$$PE_{(\text{pos}_\theta, 2i)}^r = \sin\left(\text{pos}_\theta / 10000^{\frac{2i}{d}}\right) \quad (5)$$

$$PE_{(\text{pos}_\theta, 2i+1)}^r = \cos\left(\text{pos}_\theta / 10000^{\frac{2i}{d}}\right) \quad (6)$$

$$PE_{(\text{pos}_\phi, 2i)}^r = \sin\left(\text{pos}_\phi / 10000^{\frac{2i}{d}}\right) \quad (7)$$

$$PE_{(\text{pos}_\phi, 2i+1)}^r = \cos\left(\text{pos}_\phi / 10000^{\frac{2i}{d}}\right) \quad (8)$$

where $(\text{pos}_\theta, \text{pos}_\phi)$ represents the position being computed and d represents the dimension of the positional encoding vector. This formula intricately encodes positional information by encoding each coordinate, pos_θ and pos_ϕ , to a unique 32-dimensional vector through the application of cosine and sine functions. This approach capturing the essence of spatial variations across the probability maps.

By integrating positional encoding with the original probability features, we endow the model with an enhanced capacity to recognize and interpret spatial relationships, significantly improving its performance on subsequent tasks. We feed the feature into the subsequent feature extraction module that agrees with another branch structure.

C. Multi-format Feature Fusion and Estimation Head

The features obtained from both branches are based on single frame radar data. We found that during human body movement, both the previous and subsequent frames can be used as a reference for the current frame action information. In order to make better use of the time information, we jointly process the multi-frame information. So the inherent temporal continuity of human motion is taken into account. We integrated data from multiple frames before and after the target frame, thus harnessing richer temporal features.

To integrate multi-format spatio-temporal features, we use multiple 3D convolutional layers to aggregate information. 3D convolutional blocks help extracting and consolidating features across both spatial and temporal dimensions. For each spatial scale, there is a 3D convolution block that aims to aggregate the residual uenrttemporal information. This process yields 3-layer encoded features. In addressing the challenge of integrating multi-scale features from distinct processing branches, we standardize the output dimensions of encoded features across layers. This uniformity facilitates the direct summation of positional and probability features with features from the other branch. Unlike conventional concatenation method, considering the specificity of the positional features, this direct addition method preserves spatial coherency. We obtain the fused features as:

$$F_f^i = F_1^i + F_2^i \quad (i = 1, 2, 3) \quad (9)$$

where i indicates the layers after 3D convolution. F_f represents the fused feature of each layer, and F_1, F_2 represent features from two branches.

The layer features obtained by summing go through a cross- and self-attention decoding module, which are specifically designed to enhance human pose detection by leveraging contextual information across and within the frames captured by both horizontal and vertical radar systems. The core consists of multiple decoder layers, each designed to handle features at varying scales and complexities. At each scale, the network utilizes a combination of basic 2D blocks for initial feature transformation and flatten to get an attention map in each attention system. Shown as in the lower right corner of Fig. 1, the cross-attention mechanism focuses on combining the same layer of features from both radars. In the cross-attention mechanism, we take the features from the horizontal radar as key and value, and the features from the vertical radar as query. Vice versa, switch the sources of key, query and value to perform the same operation. Since the horizontal and vertical radar capture features in different aspects, i.e. azimuth and elevation data, a residual connection is crucial to avoid directly correlating these features and ensure training stability. In addition, all key, query, and value in the self-attention system are from the same radar to enhance the internal structure of individual features. There is no skipped connections to generate self-participating residual features.

Through the attention decoding module, we obtained the predicted keypoint heatmaps from the multi-layer features. Knowing the location of some keypoints can help predict the location of other keypoints. Therefore, the pose refinement

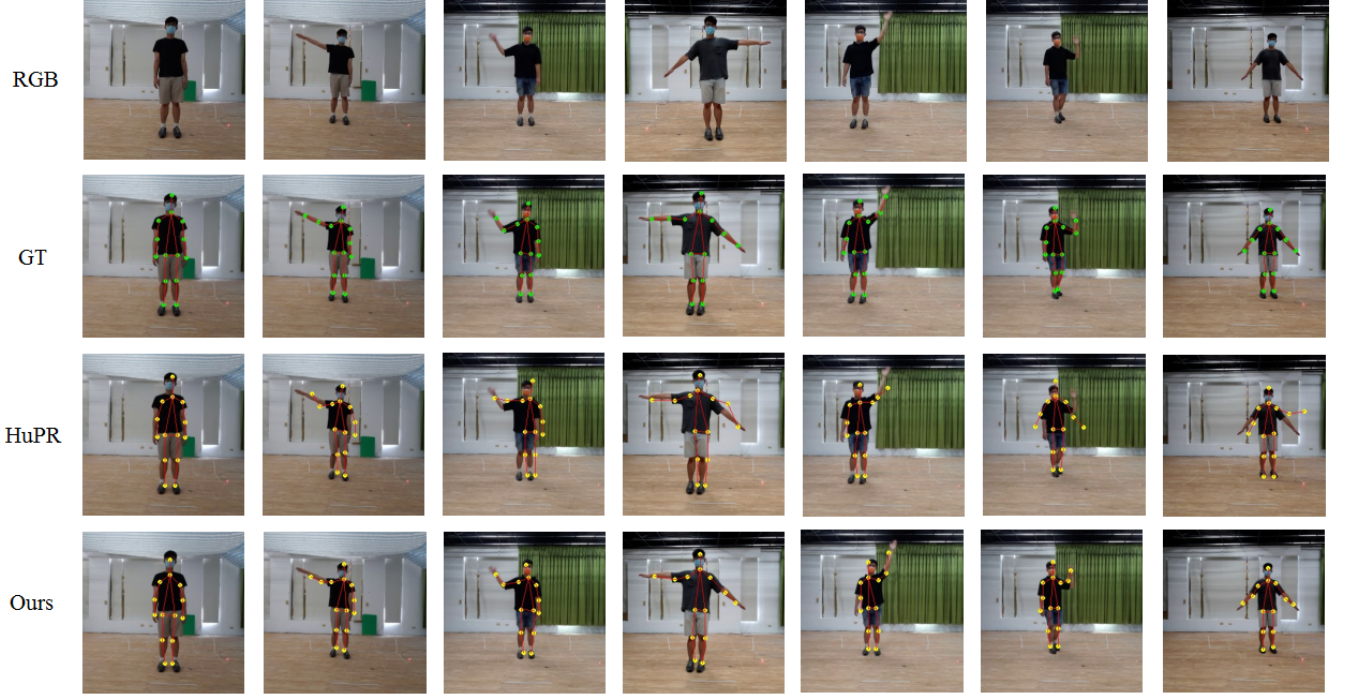


Fig. 3. Visualisation of Comparison in State-of-the-art Approaches and Our Proposed Model

module of Graph Convolutional Network (GCN) can be used to refine the keypoint heatmap [26]. We perform feature propagation and inference through a 3-layer GCN to refine the keypoint predictions using the mutual position information of the physical connections between keypoints. The generated new heatmap is used as a common reference to generate the final keypoint locations. There is a mismatch between the coordinate systems for radar signals and keypoint heatmaps, making it impossible to directly use keypoint coordinates to locate radar features. To facilitate the end-to-end training of our model, we employ a strategy of imposing a pixel-wise binary cross-entropy loss on both the initial keypoint heatmaps and the GCN-refined keypoint heatmaps. The objective function is formulated as follows:

$$L = L_{\text{bce}}(\hat{H}, G) + L_{\text{bce}}(H, G) \quad (10)$$

where H and \hat{H} represent the initial keypoint heatmaps and refined keypoint heatmaps, and G represents the generated groundtruth keypoint heatmaps based on Gaussian distribution. To illustrate, when considering the binary cross-entropy loss $L_{\text{bce}}(H, G)$, it is defined by the equation:

$$L_{\text{bce}}(H, G) = - \sum_{c,i,j} G_{c,i,j} \log(H_{c,i,j}) + (1 - G_{c,i,j}) \log(1 - H_{c,i,j}) \quad (11)$$

where c, i, j is derived from the channel, width and height of the joint prediction heatmaps H and groundtruth heatmaps G , which follow Gaussian distribution.



Fig. 4. Visualisation of Predicted Keypoints in Inaccurate Condition

IV. EXPERIMENTS AND RESULTS

A. Dataset and Evaluation

We chose the HuPR dataset for our experiments [11]. This dataset acquires data from two identical radars. One radar sensor is rotated 90° in the antenna plane with respect to the other, i.e. there is one radar sensor focusing on the horizontal plane and the other radar sensor focusing on the vertical plane. Distinguishing from some radar datasets that provide processed data in data formats such as point clouds [1, 4, 21], heatmaps [30], etc. which lose the purity of radar data, HuPR provides raw radar ADC signals. This provides more possibilities for our data processing and feature extraction methods.

TABLE I
COMPARISON OF KEYPOINT ACCURATE PRECISION

Model	AP							
	Head	Neck	Shoulder	Elbow	Wrist	Hip	Knee	Ankle
RF-Pose [36]	61.0	65.3	52.5	16.1	6.3	73.5	65.7	62.0
HuPR [11]	77.5	81.9	70.3	45.5	22.3	88.1	82.2	73.1
Ours	81.1	83.6	78.1	52.2	28.2	92.9	88.1	75.8

TABLE II
COMPARISON OF STATE-OF-THE-ART APPROACHES AND OUR PROPOSED MODEL

Model	AP	AP ⁵⁰	AP ⁷⁵
RF-Pose [36]	41.4	82.9	37.0
HuPR [11]	63.4	97.0	74.0
Ours	69.9	98.5	86.9

TABLE III
ABLATION STUDY

Model	AP	AP ⁵⁰	AP ⁷⁵
Ours(without ProbPE Branch)	66.1	97.1	79.2
Ours(without Probability Maps Generation)	67.6	98.4	84.2
Ours(Complete ProbRadarM3F Model)	69.9	98.5	86.9

The HuPR dataset provides data from 235 acquisition sequences in an indoor environment. Each sequence contains RGB camera frames, horizontal radar frames, and vertical radar frames of one minute in duration. The two radars and the camera are synchronised and configured to capture 10 frames per second (FPS), so each sequence has a ternary of 600 camera-radar-radar frames. One person in each sequence always performs a static action, a standing hand wave, and a walking hand wave. The dataset also offers groundtruth of generating by the human pose estimation network HRNet [22] from RGB frames.

In alignment with established norms in the field, our evaluation framework for 2D keypoints employs average precision (AP) metrics calculated across various levels of object keypoint similarity (OKS) [14]. The OKS are calculated as the following formula:

$$\text{OKS}_p = \frac{\sum_i \exp(-d_{p_i}^2 / 2S_p^2 \sigma_i^2) \delta(v_{p_i} = 1)}{\sum_i \delta(v_{p_i} = 1)} \quad (12)$$

where p_i denotes the id of targeted keypoint. d_{p_i} represents the Euclidean distance between the predicted keypoint and the groundtruth keypoint for the i th keypoint on person p . S_p is the scale of the person based on its area, which is calculated from the box of the person in groundtruth. σ_i is the normalisation factor of the corresponding skeletal point, reflecting the influence of the current skeletal point on the whole. $\delta(v_{p_i} = 1)$ indicates that the predicted keypoint p_i is visible in observation range.

This allows to evaluate the model's accuracy in detecting 2D keypoints across a spectrum of 14 critical human body

keypoints position, which include the head, neck, shoulders, elbows, wrists, hips, knees, and ankles. To offer a nuanced understanding of the model's performance, we use three distinct AP metrics: AP^{50} , AP^{75} , and AP . These metrics represent varying degrees of OKS stringency, with AP^{50} and AP^{75} indicating more lenient and stringent OKS constraints, respectively. The metric denoted simply as AP calculates the mean average precision across a range of 10 OKS thresholds, specifically at 0.5, 0.55, and incrementally up to 0.95, providing a comprehensive overview of the model's performance across a broad spectrum of precision requirements.

B. Implementation Details

We take 193 sequences from HuPR for training, 21 for validation, and 21 for test. The sequence are chosen as HuPR network, which is considered as baseline, for fair comparison of results.

We implement ProbRadarM3F using Python and Pytorch. The training of our network is processed on a single NVIDIA V100 GPU. The network is trained using the step decay learning rate strategy, with an initial learning rate of 0.00005 and a reduction of 0.999 times per 2000 iterations. The Adam is employed as optimizer, and we set the batch size to 24. Some other parameters in the experiment are set as follows. In CFAR processing, the settings of the guard unit and the reference unit are set to 16 and 8. The depth of positional encoding for the probability map is set to 32. The number of input frames is 8 for joint processing of multi-frame data. The convolutional of network contains basic blocks from ResNet [7]. The size of convolution kernel for 3D convolutional processing is $3 \times 3 \times 3$ and ReLU activation function is used. These parameters are selected based on optimal performance in experiments.

C. Results and Analysis

Experiments on HuPR dataset are performed to evaluate the effectiveness of the proposed strategies. Table II compares values of average precision of our proposed methods with RF-Pose [36] and baseline method [11]. ProbRadarM3F shows advantages in AP at various precision. It illustrates that our method ProbRadarM3F works much better than RF-Pose applied on the same dataset. And compared to our baseline method, which is also state of the art, our method still wins on every metric, especially on AP and AP^{75} , respectively with 6.5% and 12.9% gains. The increase in AP^{75} is a more stringent indicator that our proposed method is able to more accurately predict human keypoints. We focus on the specific

precisions of each keypoints as shown in Table I. It can be seen that our method has improved in every joint keypoint precision compared to the state of the art. The best performance is in the hip joints, where AP arrives at 92.9%. And the greatest improvement is shown in the shoulder joints, with an increase of AP of 8.2%. The reflected signals from the joints in the torso of the human body are strong and contain mass of information but little noise. So the prediction of these joints is more accurate. However, the estimation of arm and wrist joints has been a challenge in human pose estimation task due to the richer and finer arm movements and the fact that radar is less capable of capturing information from small reflective surfaces away from the torso. But our work in elbow and wrist also have 6.7% and 5.9% accuracy gains.

Fig. 3 shows the performance of our model under different types of actions in comparison. GT represents the keypoints groundtruth generated from HRNet [22] that precisely follow the actions in RGB frames, HuPR and Ours are the predictions of baseline and our ProbRadarM3F for the same frame, respectively. As can be seen, the predicted keypoints mostly follow the groundtruth. In order to show our results realistically, we also display some of the frames where the prediction is not accurate enough in Fig. 4. It can be seen that even our model loses its ability to capture details when the target is moving fast. Despite being able to predict well where the torso and head are located, there is still room for improvement at the wrist and foot joints. This observation underscores a critical area for future improvement, particularly in enhancing the model's sensitivity to high-motion extremities.

Therefore, analysing both the macroscopic overall results and the detailed individual results, our work effectively improves the precision of mmWave radar based human skeletal pose estimation. This demonstrates that the probability map guided positional encoding method is an effective mining of information contained in radar signals that might once have been overlooked.

D. Ablation Study

We conducted a series of ablation studies to evaluate the individual contributions of various components within our proposed framework, ProbRadarM3F. These studies were performed on the HuPR dataset under consistent training, validation, and testing set settings.

- To determine the impact of the ProbPE branch, we operated the network with only the FFT branch, excluding the integration of features from the positional encoding guided by probability maps. We obtain the experimental results shown in Table III. When predicting keypoints wIn the absence of the ProbPE branch, the model achieved a lower precision in keypoint prediction compared to the complete ProbRadarM3F model, particularly under stringent Object Keypoint Similarity (OKS) constraints. Specifically, excluding the ProbPE branch resulted in a decrease of 3.8% in AP and a more pronounced 7.7% reduction in AP^{75} . It is clear that the importance of ProbPE branch cannot be overstated. Obviously, the position information play a significant role to the prediction performance of the model.

- In addition to isolating the effect of the ProbPE branch as a whole, we specifically assessed the influence of probability maps in ProbPE branch. The complete model conducts positional encoding guided by probability maps, which are pivotal in generating refined positional features. To quantify the contribution of these probability maps, we conducted an ablation experiment by excluding the probability map generation step and directly applying positional encoding to the data after DOA. As shown in Table III, the precision has improved compared to using FFT branch independently, nevertheless, the absence of probability maps resulted in a noticeable decrease in performance. There is still a reduction of 2.3% in AP and 2.7%, respectively, when compared to our complete model. The results show us the importance of Probability maps. Without the guidance from the probability maps, the positional encoding becomes less effective. Consequently, the probability maps are not merely auxiliary, but integral to ensuring that the positional encoding maximally captures and utilizes the spatial context inherent in the radar signals. The probability maps enhance the model's ability to accurately determine the probability of target presence at specific azimuth and elevation coordinates, which is crucial for accurately encoding positional information.

V. CONCLUSION

In this paper, we introduce ProbRadarM3F, a novel millimetre-wave radar-based model for human skeletal pose estimation that significantly enhances the extraction and utilization of latent information from radar signals. We have innovatively designed ProbPE branch. Probability maps are generated by estimating the probability of a particular position, based on which the position features are effectively extracted from probability maps by the positional encoding method. We fused positional feature to the features obtained from the FFT branch to enrich the human body keypoint feature obtained from the model. Experiments conducted on the HuPR dataset prove that ProbRadarM3F greatly outperforms existing work, demonstrating the effectiveness of our approach. Our results show that there is still information such as mentioned position information that should not be regarded as redundant in the radar heatmap or even in the radar signal itself. There is still more information that can be introduced into the human pose estimation task from which more effective features can be captured. Looking forward, our research will continue to explore the vast potential of radar signal data. We aim to delve deeper into aspects such as motion continuity information and the fusion of multimodal data from radar heatmaps and point clouds. By expanding the scope of data utilization, we intend to capture even more effective features for human skeletal pose estimation.

REFERENCES

- [1] Sizhe An and Umit Y Ogras. Mars: mmwave-based assistive rehabilitation system for smart healthcare. *ACM Transactions on Embedded Computing Systems (TECS)*, 20(5s):1–22, 2021.

- [2] Zhongping Cao, Wen Ding, Rihui Chen, Jianxiong Zhang, Xuemei Guo, and Guoli Wang. A joint global-local network for human pose estimation with millimeter wave radar. *IEEE Internet of Things Journal*, 10(1):434–446, 2022.
- [3] Nicolas Carion, Francisco Massa, Gabriel Synnaeve, Nicolas Usunier, Alexander Kirillov, and Sergey Zagoruyko. End-to-end object detection with transformers. In *Proceedings of the 16th European Conference of Computer Vision (ECCV)*, pages 213–229, 2020.
- [4] Han Cui, Shu Zhong, Jiacheng Wu, Zichao Shen, Naim Dahnoun, and Yiren Zhao. Milipoint: A point cloud dataset for mmwave radar. *Advances in Neural Information Processing Systems*, 36, 2024.
- [5] Wen Ding, Zhongping Cao, Jianxiong Zhang, Rihui Chen, Xuemei Guo, and Guoli Wang. Radar-based 3d human skeleton estimation by kinematic constrained learning. *IEEE Sensors Journal*, 21(20):23174–23184, 2021.
- [6] Xu Feng, Khuong An Nguyen, and Zhiyuan Luo. A survey of deep learning approaches for wifi-based indoor positioning. *Journal of Information and Telecommunication*, 6(2):163–216, 2022.
- [7] Kaiming He, Xiangyu Zhang, Shaoqing Ren, and Jian Sun. Deep residual learning for image recognition. In *Proceedings of the IEEE conference on Computer Vision and Pattern Recognition (CVPR)*, pages 770–778, 2016.
- [8] Tao Huang, Jianan Liu, Xi Zhou, Dinh C Nguyen, Mostafa Rahimi Azghadi, Yuxuan Xia, Qing-Long Han, and Sumei Sun. V2x cooperative perception for autonomous driving: Recent advances and challenges. 2023. *arXiv:2310.03525*.
- [9] Cesar Iovescu and Sandeep Rao. The fundamentals of millimeter wave sensors. *Texas Instruments*, pages 1–8, 2017.
- [10] Hao Kong, Xiangyu Xu, Jiadi Yu, Qilin Chen, Chenguang Ma, Yingying Chen, Yi-Chao Chen, and Linghe Kong. m3track: mmwave-based multi-user 3d posture tracking. In *Proceedings of the 20th Annual International Conference on Mobile Systems, Applications and Services*, pages 491–503, 2022.
- [11] Shih-Po Lee, Niraj Prakash Kini, Wen-Hsiao Peng, Ching-Wen Ma, and Jenq-Neng Hwang. Hupr: A benchmark for human pose estimation using millimeter wave radar. In *Proceedings of the IEEE/CVF Winter Conference on Applications of Computer Vision (WACV)*, pages 5715–5724, 2023.
- [12] Qimeng Li, Jikui Liu, Raffaele Gravina, Weilin Zang, Ye Li, and Giancarlo Fortino. A uwb-radar-based adaptive method for in-home monitoring of elderly. *IEEE Internet of Things Journal*, 11(4):6241–6252, 2024.
- [13] Zhi Li, Tian Jin, Dongfang Guan, and Hantao Xu. Metaphys: Contactless physiological sensing of multiple subjects using ris-based 4-d radar. *IEEE Internet of Things Journal*, 10(14):12616–12626, 2023.
- [14] Tsung-Yi Lin, Michael Maire, Serge Belongie, James Hays, Pietro Perona, Deva Ramanan, Piotr Dollár, and C Lawrence Zitnick. Microsoft coco: Common objects in context. In *Proceedings of the 13th European Conference of Computer Vision (ECCV)*, pages 740–755, 2014.
- [15] Jianan Liu, Guanhua Ding, Jinping Xia, Yuxuan Sun, Tao Huang, Lihua Xie, and Bing Zhu. Which framework is suitable for online 3D multi-object tracking for autonomous driving with automotive 4D imaging radar? In *Proceedings of the IEEE 35th Intelligent Vehicles Symposium (IV)*, 2024. *arXiv:2309.06036*.
- [16] Jianan Liu, Weiyi Xiong, Liping Bai, Yuxuan Xia, Tao Huang, Wanli Ouyang, and Bing Zhu. Deep instance segmentation with automotive radar detection points. *IEEE Transactions on Intelligent Vehicles*, 8(1):84–94, January 2023.
- [17] Jianan Liu, Qiuchi Zhao, Weiyi Xiong, Tao Huang, Qing-Long Han, and Bing Zhu. SMURF: Spatial multi-representation fusion for 3D object detection with 4D imaging radar. *IEEE Transactions on Intelligent Vehicles*, 9(1):799–812, October 2024.
- [18] Mario Pauli, Benjamin Göttel, Steffen Scherr, Akanksha Bhutani, Serdal Ayhan, Wolfgang Winkler, and Thomas Zwick. Miniaturized millimeter-wave radar sensor for high-accuracy applications. *IEEE transactions on microwave theory and techniques*, 65(5):1707–1715, 2017.
- [19] Mark A Richards, Jim Scheer, William A Holm, and William L Melvin. Principles of modern radar. 2010.
- [20] Arindam Sengupta, Feng Jin, Renyuan Zhang, and Siyang Cao. mm-pose: Real-time human skeletal posture estimation using mmwave radars and cnns. *IEEE Sensors Journal*, 20(17):10032–10044, 2020.
- [21] Akash Deep Singh, Sandeep Singh Sandha, Luis Garcia, and Mani Srivastava. Radhar: Human activity recognition from point clouds generated through a millimeter-wave radar. In *Proceedings of the 3rd ACM Workshop on Millimeter-wave Networks and Sensing Systems*, pages 51–56, 2019.
- [22] Ke Sun, Bin Xiao, Dong Liu, and Jingdong Wang. Deep high-resolution representation learning for human pose estimation. In *Proceedings of the IEEE/CVF Conference on Computer Vision and Pattern Recognition (CVPR)*, pages 5693–5703, 2019.
- [23] Bram van Berlo, Amany Elkellany, Tanir Ozcelebi, and Nirvana Meratnia. Millimeter wave sensing: A review of application pipelines and building blocks. *IEEE Sensors Journal*, 21(9):10332–10368, 2021.
- [24] Ashish Vaswani, Noam Shazeer, Niki Parmar, Jakob Uszkoreit, Llion Jones, Aidan N Gomez, Łukasz Kaiser, and Illia Polosukhin. Attention is all you need. *Advances in neural information processing systems*, 30, 2017.
- [25] Haoyu Wang, Jinbo Chen, Dongheng Zhang, Zhi Lu, Changwei Wu, Yang Hu, Qibin Sun, and Yan Chen. Contactless radar heart rate variability monitoring via deep spatio-temporal modeling. In *IEEE International Conference on Acoustics, Speech and Signal Processing (ICASSP)*, pages 111–115, 2024.
- [26] Jian Wang, Xiang Long, Yuan Gao, Errui Ding, and Shilei Wen. Graph-pcnn: Two stage human pose estimation with graph pose refinement. In *Proceedings of the 16th European Conference of Computer Vision (ECCV)*, pages 492–508, 2020.
- [27] Yizhou Wang, Zhongyu Jiang, Yudong Li, Jenq-Neng Hwang, Guanbin Xing, and Hui Liu. Rodnet: A real-time radar object detection network cross-supervised by camera-radar fused object 3d localization. *IEEE Journal of Selected Topics in Signal Processing*, 15(4):954–967, 2021.
- [28] Zhengjie Wang, Xue Li, Fei Liu, Mingjing Ma, Xiaoxue Feng, and Yinjing Guo. A survey on human behavior recognition applications using frequency modulated continuous wave radar. In *Proceedings of the 2022 10th International Conference on Information Technology: IoT and Smart City*, pages 133–139, 2022.
- [29] Zhi Wu, Dongheng Zhang, Chunyang Xie, Cong Yu, Jinbo Chen, Yang Hu, and Yan Chen. Rfmask: A simple baseline for human silhouette segmentation with radio signals. *IEEE Transactions on Multimedia*, 2022.
- [30] Chunyang Xie, Dongheng Zhang, Zhi Wu, Cong Yu, Yang Hu, and Yan Chen. Rpm: Rf-based pose machines. *IEEE Transactions on Multimedia*, 2023.
- [31] Weiyi Xiong, Jianan Liu, Tao Huang, Qing-Long Han, Yuxuan Xia, and Bing Zhu. LXL: LiDAR excluded lean 3D object detection with 4D imaging radar and camera fusion. *IEEE Transactions on Intelligent Vehicles*, 9(1):79–92, October 2024.
- [32] Weiyi Xiong, Jianan Liu, Yuxuan Xia, Tao Huang, Bing Zhu, and Wei Xiang. Contrastive learning for automotive mmWave radar detection points based instance segmentation. In *Proceedings of the IEEE 25th International Conference on Intelligent Transportation Systems (ITSC)*, pages 1255–1261, 2022.
- [33] Yanlong Yang, Jianan Liu, Tao Huang, Qing-Long Han, Gang Ma, and Bing Zhu. RaLiBEV: Radar and LiDAR BEV fusion learning for anchor box free object detection systems. 2022. *arXiv:2211.06108*.
- [34] Hongwei Yi, Chen Li, Qiong Cao, Xiaoyong Shen, Sheng Li, Guoping Wang, and Yu-Wing Tai. Mmface: A multi-metric

- regression network for unconstrained face reconstruction. In *Proceedings of the IEEE/CVF conference on computer vision and pattern recognition*, pages 7663–7672, 2019.
- [35] Jia Zhang, Rui Xi, Yuan He, Yimiao Sun, Xiuzhen Guo, Weiguo Wang, Xin Na, Yunhao Liu, Zhenguo Shi, and Tao Gu. A survey of mmwave-based human sensing: Technology, platforms and applications. *IEEE Communications Surveys & Tutorials*, 2023.
- [36] Mingmin Zhao, Tianhong Li, Mohammad Abu Alsheikh, Yonglong Tian, Hang Zhao, Antonio Torralba, and Dina Katabi. Through-wall human pose estimation using radio signals. In *Proceedings of the IEEE conference on computer vision and pattern recognition*, pages 7356–7365, 2018.
- [37] Zhijie Zheng, Jun Pan, Zhikang Ni, Cheng Shi, Shengbo Ye, and Guangyou Fang. Human posture reconstruction for through-the-wall radar imaging using convolutional neural networks. *IEEE Geoscience and Remote Sensing Letters*, 19:1–5, 2021.